Nano Energy 44 (2018) 311–318

Contents lists available at ScienceDirect

Nano Energy

journal homepage: www.elsevier.com/locate/nanoen

Full paper

Enhanced performances of Si/CdS heterojunction near-infrared photodetector by the piezo-phototronic effect

Yejing Dai[a,b,1], Xingfu Wang[a,1], Wenbo Peng[a,c,1], Changsheng Wu[a], Yong Ding[a], Kai Dong[a], Zhong Lin Wang[a,d,*]

[a] School of Materials Science and Engineering, Georgia Institute of Technology, Atlanta, GA 30332-0245, United States
[b] Key Laboratory of Advanced Ceramics and Machining Technology, Ministry of Education, School of Materials Science and Engineering, Tianjin University, Tianjin 300072, China
[c] School of Electronic and Information Engineering, Xi'an Jiaotong University, Xi'an 710049, China
[d] Beijing Institute of Nanoenergy and Nanosystems, Chinese Academy of Sciences, Beijing 100083, China

ARTICLE INFO

Keywords:
Piezo-phototronic effect
Heterojunction
Near-infrared
Photodetector
Si-based

ABSTRACT

Owing to the compatibility with the traditional integrated circuit technology, it is of great significance to enhance the photoresponse performance of Silicon (Si)-based photodetectors (PDs) in the near-infrared (NIR) wavelength. Here, by introducing the piezo-phototronic effect, the photoresponsivity and the specific detectivity of the p-Si/n-CdS heterojunction NIR PD are enhanced by 966 times and two orders of magnitude with a 1064 nm illumination of 0.35 mW cm^{-2} power density under -0.50‰ compressive strain, which is even better than those of commercial Si PDs. The piezo-phototronic effect is a three-way coupling effect of piezoelectricity, semiconductor and optical excitation in piezoelectric semiconductors, such as wurtzite structured CdS. Alternatively, the performance enhancement of the n-Si/n-CdS heterojunction PD by the piezo-phototronic effect is much less than that of the p-n heterojunction PD under the same compressive straining conditions, due to their different energy band structures near the Si/CdS heterojunction. This work provides not only a facile solution-processed fabrication for high-performance Si-based NIR PDs, but also a deep understanding about the piezo-phototronic effect on the performance enhancement of Si/CdS heterojunction NIR PDs.

1. Introduction

Silicon (Si)-based optoelectronic devices are good candidates for monolithic integration with complementary metal-oxide semiconductor (CMOS) readout circuitry due to their excellent compatibility [1,2]. Until now, the combination of silicon and nanostructure has developed a series of new optoelectronic devices, such as photodetectors (PDs) [3,4], solar cell [5,6], and light emitter [7–9]. Among them, nanostructure-based PDs with broadband response range and high sensitivity have aroused much attention for integrated optoelectronic applications, *e.g.* optical communication, imaging and sensor networks [10–15]. However, due to its indirect bandgap, traditional Si p-n junction PDs have low light absorption in near-infrared (NIR) wavelength and thus low photoresponsivity, which limits the development of broadband detection using Si-based materials [16]. In addition, traditional Si-based PDs suffer from a complicated fabrication process [17,18]. Therefore, it is important to develop a simple and cost-effective way for high-performance Si-based NIR PDs with improved photoresponse.

Piezoelectric semiconductors with non-centrosymmetric structure, such as wurtzite-structured ZnO, GaN and CdS, can produce piezoelectric polarization charges at the polar ends of the semiconductor crystal upon externally applied strain [19–21]. The strain-induced piezoelectric polarization charges at the local homo-/hetero-junction interface will tune the energy band of the heterojunction near the interface, and therefore modulate the generation, transport and/or recombination of photo-generated carriers at the interface, which is referred to as the piezo-phototronic effect [22–27].

In this work, *via* a simple hydrothermal synthesis, we fabricated two kinds of Si/CdS heterojunction PDs (*i.e.* p-Si/n-CdS and n-Si/n-CdS heterojunctions). By introducing the piezo-phototronic effect, the photoresponse performances of both heterojunction PDs in the NIR band are enhanced. For the p-Si/n-CdS heterojunction PD, a photoresponsivity R of 14.5 A W^{-1} corresponding to an increase of 966 times and a detectivity D^* of 1.65 × 10^{12} Jones corresponding to an enhancement of two orders of magnitude, were obtained under an externally applied compressive strain of -0.50‰, accompanied by

* Corresponding author at: School of Materials Science and Engineering, Georgia Institute of Technology, Atlanta, Georgia 30332-0245, United States.
E-mail address: zhong.wang@mse.gatech.edu (Z.L. Wang).
[1] These authors contributed equally to this work.

https://doi.org/10.1016/j.nanoen.2017.11.076
Received 31 October 2017; Received in revised form 26 November 2017; Accepted 30 November 2017
Available online 05 December 2017

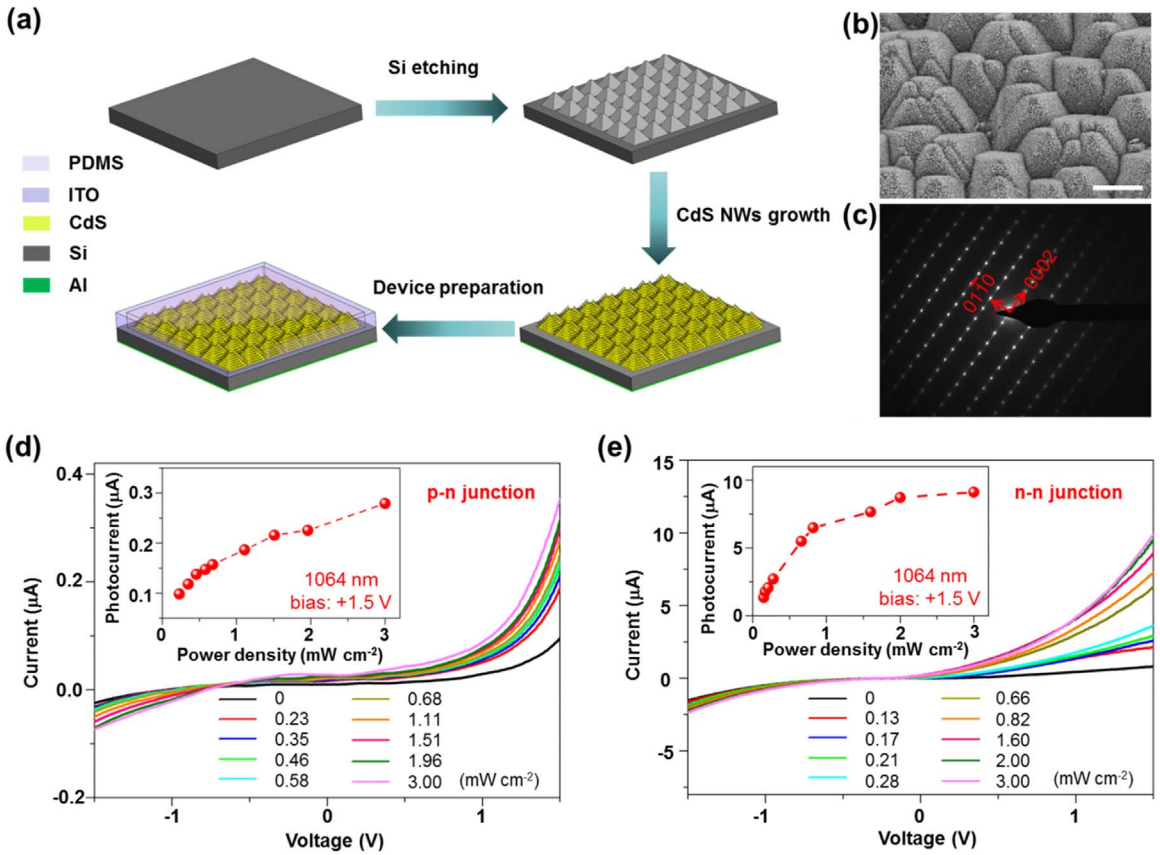

Fig. 1. Fabrication process, structure, characterization and properties of the heterojunction NIR PDs. (a) Fabrication process and schematic structure of a Si/n-CdS NWs heterostructure NIR PD. (b) SEM image of the CdS NW array synthesized on the etched Si wafer. The scale bar is 10 μm. (c) The select area electron diffraction pattern of a CdS NW. (d, e) *I-V* characteristics under different 1064 nm illumination power densities when a 1.5 V bias is applied for the p-n junction (d) and n-n junction (e) PDs, respectively. The insets show the photocurrent changes with the power density at 1.5 V forward bias.

drastically reduced response time. On the other hand, for the n-Si/n-CdS heterojunction PD, a photoresponsivity R of 2.62 A W^{-1} corresponding to only an increase of 6 times, as well as a slightly improved detectivity D^* of 2.55 × 10^{11} Jones, was obtained under the same externally applied compressive strain. The different influences of externally applied compressive strain on the two kinds of Si/CdS heterojunction PDs are attributed to the different energy band structures of the p-Si/n-CdS and n-Si/n-CdS heterojunctions. These results provide a facile and effective way to enhance the photoresponse capability of Si-based materials in the NIR band by the piezo-phototronic effect, and in-depth understanding about the piezo-phototronic effect on the two different kinds of heterojunction PDs.

2. Results and discussion

2.1. Structure and photoresponse performances of the Si/CdS heterojunction NIR PDs

The fabrication process and the structure of the Si/CdS heterojunction NIR PDs are schematically illustrated in Fig. 1a. First, the smooth surface of a polished Si wafer was etched into many small tetrahedrons with the bottom edge length of 3–10 μm by KOH solution in order to increase the light absorption area (Fig. S1a in Supporting Information). Then, by a facile hydrothermal synthesis process, CdS NWs with an average diameter of 50 nm and an average length of 600 nm were perpendicularly grown on the surfaces of Si tetrahedrons (Fig. 1b and S1b), confirmed by the select-area electron diffraction (SAED) pattern from a single CdS NW (Fig. 1c). The transmission spectrum of CdS NW array grown on the FTO/glass substrate shows a good light transmission in the NIR band (Fig. S2 in Supporting Information). Finally, the top and bottom electrodes were deposited. Detailed fabrication process and measurement setup are described in Experimental methods and Fig. S3 in Supporting Information.

The photoresponse behavior of the Si/CdS heterojunction NIR PDs with p-n and n-n junctions are displayed in Fig. 1d and e by applying 1064 nm laser illumination, respectively. For the p-n junction PD, with increasing laser power density from 0 to 3 mW cm^{-2}, the photocurrent under 1.5 V forward bias increases from 0.10 to 0.28 μA with an increase of 2.8 times, as shown in the inset of Fig. 1d. However, for the n-n junction PD, the photocurrent under the same bias increases from 1.35 to 9.11 μA with an increase of 6.7 times, as shown in the inset of Fig. 1e. The calculated photoresponsivity R is 4.1 mA W^{-1} for the p-Si/n-CdS heterojunction PD and it is 135.3 mA W^{-1} for the n-Si/n-CdS heterojunction PD at a power density of 3 mW cm^{-2}. Here, R is defined as:

$$R = \frac{\Delta I}{I_{ill} \times S},$$

where $\Delta I = I_{light} - I_{dark}$ (I_{light} and I_{dark} are the output currents with and without laser illumination), I_{ill} is the power density, S is the effective area of the PD [28]. These results indicate that, under the strain-free condition with the same incident power density, the n-Si/n-CdS heterojunction PD has much better photoresponse performance compared with the p-Si/n-CdS heterojunction PD at 1.5 V forward bias.

2.2. Piezo-phototronic effect on photoresponse performances

To compare the piezo-phototronic effect on the two different heterojunction NIR PDs, the photoresponse performances of the NIR PDs with laser power density from 0 to 3 mW cm^{-2} under six different

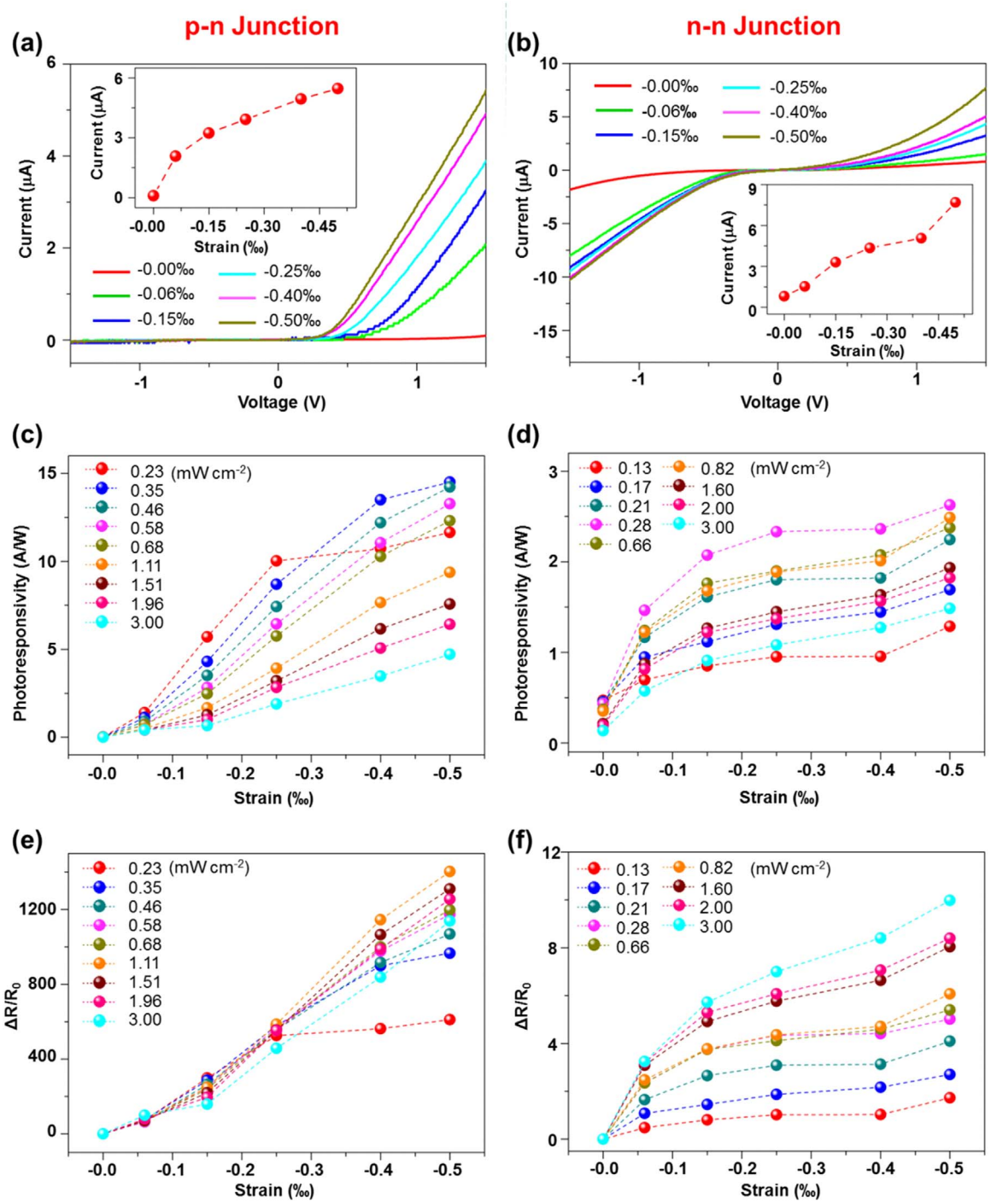

Fig. 2. The piezo-phototronic effect on the Si/CdS heterojunction NIR PDs. (a, b) *I-V* characteristics under different compressive strains without laser illumination for p-n (a) and n-n (b) junction PDs, respectively. The insets show the output current changes with the external compressive strain at 1.5 V forward bias. (c, d) Photoresponsivity *R* under different compressive strains and illumination conditions when the forward bias is 1.5 V for p-n (c) and n-n (d) junction PDs, respectively. (e, f) Relative changes $\Delta R/R_0$ of photoresponsivity under different compressive strains and illumination conditions when the forward bias is 1.5 V for p-n (e) and n-n (f) junction PDs, respectively.

externally applied compressive strains are measured, summarized and shown in Fig. 2. First, the *I-V* characteristics of the p-n (Fig. 2a) and n-n (Fig. 2b) junction PDs under six different externally applied compressive strains without laser illumination were investigated, respectively. For the p-n junction PD, it is clear that, with increasing compressive strain, the output current at 1.5 V forward bias increases from 0.10 to 5.47 μA, whereas there is no obvious change for the output currents at 1.5 V reverse bias. For the n-n junction PD, the output current at 1.5 V forward bias increases from 0.82 to 7.70 μA, accompanied by an increase in the output current at 1.5 V reverse bias from −1.84 to −10.30 μA. These results indicate that the externally applied compressive strain could effectively adjust the output current at 1.5 V forward bias for both heterojunction PDs. Then, by applying 1064 nm laser illumination with nine different power densities, the *I-V* characteristics of the Si/CdS NWs heterojunction PDs under six different externally applied compressive strains were measured, and the corresponding photocurrents ΔI at 1.5 V forward bias were calculated and displayed in Fig. S4a and b, respectively. At a certain power density, the photocurrent increases with the externally applied compressive strain. For example, when the externally applied compressive strain changes from

-0.00‰ to -0.50‰, the photocurrent of the PD with p-n junction under 3.00 mW cm^{-2} laser illumination increases from 0.28 to 318.2 μA, whereas that of the PD with n-n junction under the same laser illumination increases from 9.12 to 99.2 μA, indicating that the photoresponse performances of the two heterojunction NIR PDs are significantly enhanced by the piezo-phototronic effect.

Based on the value of the photocurrent, the photoresponsivity R and specific detectivity D^* of the two heterojunction NIR PDs under different power densities and externally applied compressive strains at 1.5 V forward bias are calculated and shown in Fig. 2c, d, S4c and S4d, respectively. D^* is defined as $D^* = \frac{R}{\sqrt{2qJ_d}}$, where q is the elemental charge, and J_d is the dark current density [28]. For the p-n junction PD, a gradual increase in R and D^* with increasing externally applied compressive strain was observed (Fig. 2c and S4c) for each power density. When applying a -0.50‰ strain to the p-n junction PD, a maximum R of 14.5 A W^{-1} and a maximum D^* of 1.65 × 10^{12} Jones could be obtained with the power density of 0.35 mW cm^{-2}, whereas the R is only 0.015 A W^{-1} and the D^* is only 1.29 × 10^{10} Jones under the strain-free condition. These enhanced performances are impressive and competitive with other reported Si-based nanostructure NIR PDs and commercial Si photodiodes (0.1 ~ 0.3 A W^{-1} at 1100 nm) [29–33]. To better illustrate the piezo-phototronic effect on the R, the relative changes of R for the p-n and n-n junction NIR PDs defined as $\Delta R/R_0$ ($\Delta R = R_s$-R_0, where R_s is the R under a certain compressive strain, and R_0 is the R under the strain-free condition) for each power density are calculated and shown in Fig. 2e and f, respectively. For the p-n junction PD, $\Delta R/R_0$ increases with externally applied compressive strain (Fig. 2e), and it is 966 at a power density of 0.35 mW cm^{-2} under − 0.50‰ compressive strain. The maximum $\Delta R/R_0$ of 1402 can be achieved by applying − 0.50‰ compressive strain when power density is 1.11 mW cm^{-2}, indicating that the piezoelectric polarization charges (piezo-charges) induced by the externally applied compressive strain have a significant effect on the interface of the energy band of the p-n junction PD. Similar results are found in the n-n junction PD, and the R, D^* and $\Delta R/R_0$ also increase as the externally applied compressive strain increases. The maximum R of 2.62 A W^{-1} and D^* of 2.55 × 10^{11} Jones could be obtained under − 0.50‰ compressive strain with a power density of 0.28 mW cm^{-2}, while the R is 0.44 A W^{-1} and the D^* is 1.29 × 10^{11} Jones under the strain-free condition. The maximum $\Delta R/R_0$ value is 10 by applying − 0.50‰ compressive strain when the power density is 3.00 mW cm^{-2}. Therefore, the performance enhancement of the p-n junction PD by the piezo-phototronic effect is much larger than that of the n-n junction PD.

The repeatability and time-dependent responses of the p-n and n-n junction PDs under different compressive strains and 1064 nm laser illumination with a power density of 3 mW cm^{-2} at 1.5 V forward bias are presented in Fig. 3a and b, respectively. The responses show good repeatability and consistency under all compressive strains. The rise time (defined as the time taken for the current increasing from 10% to 90% of maximum photocurrent) and fall time (defined as the time taken for the current decreasing from 90% to 10% of maximum photocurrent) [34,35] of the p-n and n-n junction PDs are calculated based on the curves in Fig. 3a and b, and plotted in Fig. 3c and d, respectively. Interestingly, the rise time and fall time of the p-n junction PD both reduced with increasing compressive strain. The rise time decreases from 141.7 to 19.7 ms, and the fall time decreases from 22.0 to 13.9 ms, as shown in Fig. 3c. However, for the n-n junction PD, the rise time only has a slight decrease from 13.4 to 12.8 ms and the fall time keeps almost unchanged with increasing compressive strain (Fig. 3d). The different influences of the externally applied compressive strain on the photoresponse performance and response speed of the p-n and n-n junction PDs may be attributed to the different energy band structures near the Si/CdS interface.

2.3. Working mechanism of the piezo-phototronic effect

Fig. 4a shows a schematic structure model of the Si/CdS heterojunction under externally applied compressive stress, showing the piezoelectric potential (piezo-potential) distribution within the CdS NW. As the CdS NWs grow vertically on the surface of Si along the c-axis, the positive piezo-charges are created at the -c end of CdS NW under externally applied compressive stress. Simultaneously, the negative piezo-charges are created at the +c end of CdS NW, which is equivalent to an extra forward bias on the Si/CdS heterojunction PD. The calculation of the external compressive strain applied on CdS NWs and the piezo-potential distribution at the interface of Si/CdS NWs heterojunction under compressive strain were conducted *via* finite element analysis (FEA) method. Considering that the simulation and calculation would be very complicated if the actual 3D dimensions of the Si/CdS NWs heterojunction NIR PDs are used as the simulation model, a simplified two dimensional (2D) model of the Si/CdS NWs heterojunction PD was built and the piezo-potential distribution is shown in Fig. S5a. Fig. S5b shows that, under externally applied compressive strain, positive piezo-potential is induced along the arc-length (purple line in Fig. S5a) at the local interface of the Si/CdS NWs heterojunction. The closer to the upper part of the tetrahedron, the higher the piezo-potential is. More detailed information about the simulation and calculation could be found in Experimental methods and Supporting Information (Supplementary Note 1).

The effect of the externally applied compressive strain on the carrier transportation at the Si/CdS interface can be illustrated from the energy band diagrams of p-Si/n-CdS and n-Si/n-CdS heterojunction PDs, respectively (Fig. 4b–e). The band gap and electron affinity of Si and CdS are $E_{g,Si}$ = 1.12 eV, χ_{Si} = 4.05 eV [36] and $E_{g,CdS}$ = 2.42 eV, χ_{CdS} = 4.40 eV [37], respectively. Once a Si/CdS heterojunction is formed, a conduction band offset ΔE_c = 0.35 eV and a valence band offset ΔE_v = 1.65 eV are formed at the interface for both the p-Si/n-CdS and n-Si/n-CdS heterojunction PDs according to Anderson's model [38]. When the two heterojunction PDs are under the strain-free condition at 0 V bias, different energy band diagrams as well as depletion regions would be formed at the local Si/CdS interfaces according to the different dopants of the Si for p-Si/n-CdS and n-Si/n-CdS heterojunctions, as shown in Fig. 4b and d, respectively. Depletion regions are formed at both Si and CdS sides for the p-Si/n-CdS heterojunction, whereas it is only formed at the Si side for the n-Si/n-CdS heterojunction. Therefore, for the p-Si/n-CdS heterojunction under the strain-free condition at +1.5 V forward bias (black dotted line in Fig. 4c), the energy bands (E_c and E_v) at the p-Si side near the local interface change from downward to upward, indicating the hole accumulation due to the formation of a potential well at the p-Si side near the local Si/CdS interface (marked in Fig. 4c). Moreover, the energy bands (E_c and E_v) are tilted at the n-CdS side, which means that the forward bias is mainly applied at the n-CdS side. While for the n-Si/n-CdS heterojunction under the strain-free condition at + 1.5 V forward bias (black dotted line in Fig. 4e), the forward bias is mainly applied at the n-Si side as the depletion region is only formed at the n-Si side, which also significantly expands the depletion region at the n-Si side, as shown in Fig. 4e. As a result, the energy bands at the n-CdS side keep almost unchanged. In short, under the strain-free condition at + 1.5 V forward bias, a hole accumulation region is formed at the p-Si side for the p-Si/n-CdS heterojunction while an expanded depletion region is formed at the n-Si side for the n-Si/n-CdS heterojunction. Considering that the photo-generated carriers are mainly produced at the Si side for both p-Si/n-CdS and n-Si/n-CdS heterojunctions, therefore, the n-Si/n-CdS heterojunction PD has much better photoresponse (R ~ 135.3 mA W^{-1}) than that (R ~ 4.1 mA W^{-1}) of the p-Si/n-CdS heterojunction PD under the strain-free condition, because the effective region for generating and separating photo-generated carriers at the n-Si side in the n-Si/n-CdS heterojunction PD is much larger compared to that of the p-Si/n-CdS heterojunction PD.

Once the external compressive strain is applied, positive piezo-

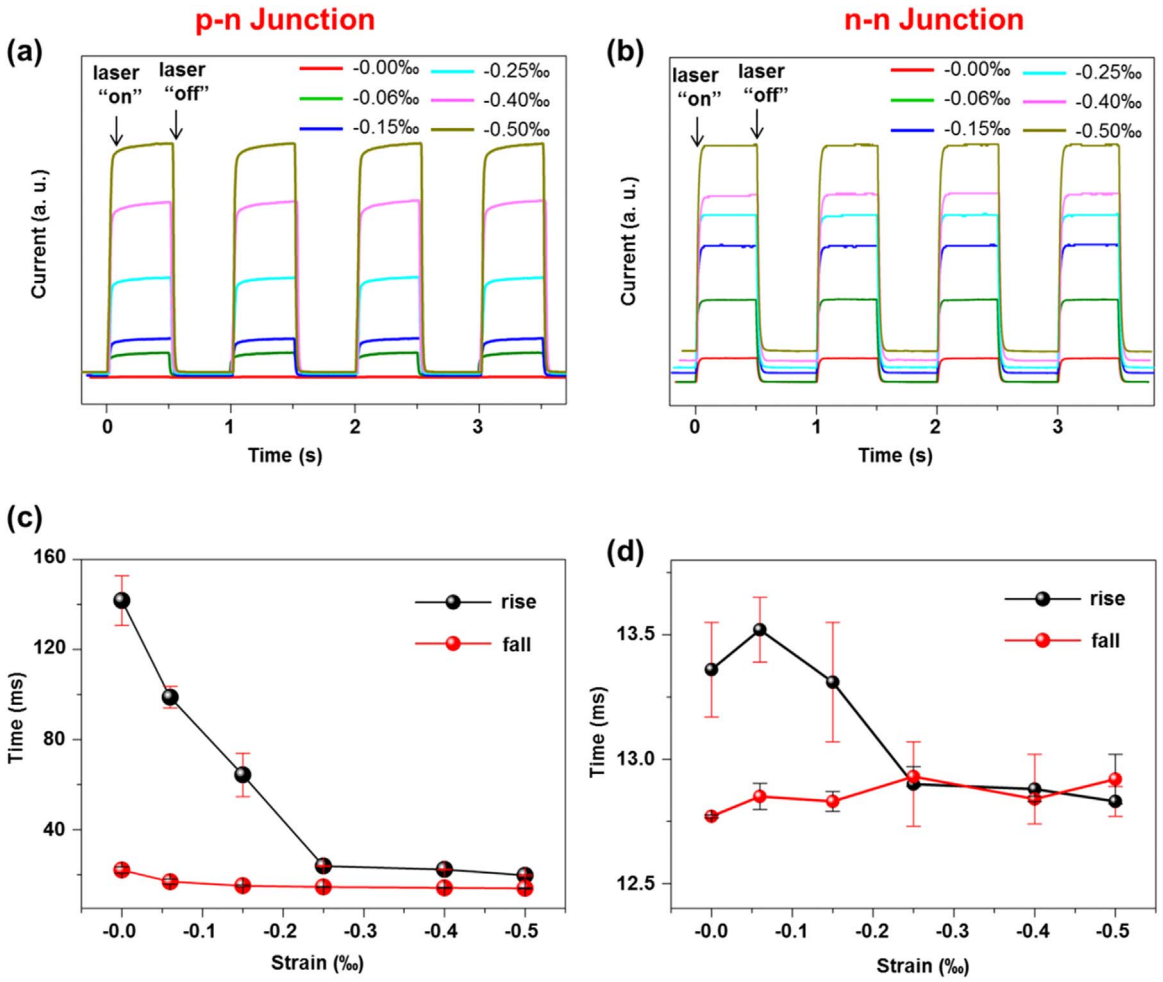

Fig. 3. Repeatability and response speed of the heterojunction NIR PDs. (a, b) Time response and repeatability for different compressive strains under 1064 nm illumination with a power density of 3 mW cm^{-2} for p-n (a) and n-n (b) junction PDs, respectively. (c, d) The corresponding rise time and fall time under different compressive strains for p-n (c) and n-n (d) junction PDs, respectively.

charges are induced and distributed at the local Si/CdS interfaces due to the polar *c*-axis growth direction of the CdS NWs. As the direction of the piezoelectric potential generated by the externally applied compressive strain is consistent with that of the applied forward bias, the output current is expected to be enhanced when the heterojunction PDs are under the compressive strain condition, indicating that the photoresponse performances of the NIR PDs based on p-Si/n-CdS and n-Si/n-CdS heterojunctions would be both enhanced by the piezo-phototronic effect. For the p-Si/n-CdS heterojunction under the compressive strain condition at +1.5 V forward bias, the positive piezo-charges repel the holes away from the local Si/CdS interface at the p-Si side and attract the electrons moving toward the local Si/CdS interface at the n-CdS side, resulting in a downward bending of the energy band diagram of both p-Si and n-CdS sides (dark yellow line in Fig. 4c). Consequently, the effect of the potential well at the p-Si side near the local Si/CdS interface (marked in Fig. 4c) on the photo-generated hole confinement would be weakened under the compressive strain condition compared to that under the strain-free condition, leading to increased photo-generated hole current and thus the improved photoresponse performance of the p-Si/n-CdS heterojunction NIR PD. Meanwhile, the photo-generated electrons can still be easily driven towards and collected by the anode due to the upward bending of the conduction band at the p-Si side.

For the n-Si/n-CdS heterojunction PD under the compressive strain condition at + 1.5 V forward bias, the positive piezo-charges will attract the electrons moving toward the local Si/CdS interface at both the n-Si and n-CdS sides, also resulting in a downward bending of the energy band diagram of both n-Si and n-CdS sides (dark yellow line in Fig. 4e). As a result, the potential well at the n-Si side near the local Si/CdS interface (marked in Fig. 4e) becomes shallower and thinner under the compressive strain condition compared to that under the strain-free condition, leading to the weakened confinement of the photo-generated holes and thus the enhanced photoresponse performance of the n-Si/n-CdS heterojunction NIR PD. Moreover, it is noteworthy that energy bands (E_c and E_v) at the n-CdS side are tilted under the compressive strain condition, also contributing to the collection of photo-generated holes and therefore the enhancement of photoresponse performances of the n-Si/n-CdS heterojunction NIR PD. However, as the electrons are attracted at the n-Si side of the local Si/CdS interface due to the positive piezo-charges, the depletion region width at the n-Si side is significantly shortened as illustrated in Fig. 4e, which greatly reduces the generation and separation of photo-generated carriers in the n-Si side and hence the photoresponse performances of the n-Si/n-CdS heterojunction NIR PD. Considering all the energy band diagram's changes and corresponding consequences caused by the positive piezo-charges, the enhancement of the photoresponse performance of the n-Si/n-CdS heterojunction PD is smaller than that of the p-Si/n-CdS heterojunction PD under the same compressive strain condition, meaning that the externally applied compressive strain has a relatively small impact on the photoresponse (Fig. 2f) and response speed (Fig. 3d) of the n-Si/n-CdS heterojunction PD when compared to the p-Si/n-CdS heterojunction PD. The working mechanisms of these two heterojunction NIR PDs are

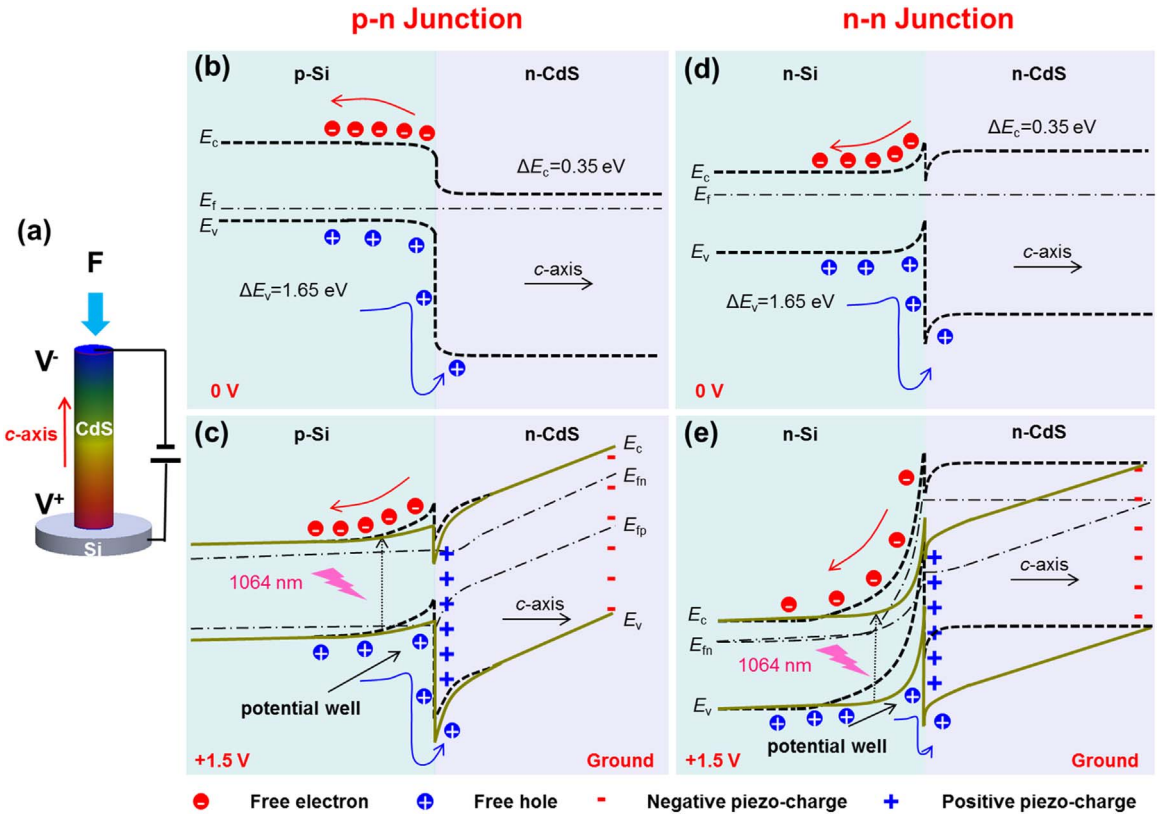

Fig. 4. Working mechanism of the heterostructure NIR PDs by the piezo-phototronic effect. (a) A schematic structure model of the Si/CdS heterojunction with the piezoelectric potential distribution under compressive stress. (b, c) Schematic band diagrams of a p-Si/n-CdS p-n junction without (black dotted line) and with (dark yellow line) a compressive strain under 0 V forward bias (b) and under 1.5 V forward bias (c). (d, e) Schematic band diagrams of an n-Si/n-CdS n-n junction without (black dotted line) and with (dark yellow line) a compressive strain under 0 V forward bias (d) and under 1.5 V forward bias (e). (For interpretation of the references to color in this figure legend, the reader is referred to the web version of this article.)

also confirmed by the calculated band diagrams *via* FEA method for different compressive strains at +1.5 V forward bias, shown in Figs. S6 and S7, and the details about the FEA simulation are found in Supporting Information (Supplementary Note 2). The simulated energy band diagrams are modulated under compressive strains, thus affecting the carrier transport properties of the two heterojunction NIR PDs.

3. Conclusions

In summary, we have fabricated two kinds of Si/CdS heterojunction NIR PDs (p-Si/n-CdS and n-Si/n-CdS), and improved the photoresponse performances of both Si/CdS heterojunction NIR PDs in the NIR band by the piezo-phototronic effect. Under the strain-free condition, the photoresponse performance of the n-n junction PD is much better than that of the p-n junction PD, both of which are enhanced under externally applied compressive strain by the piezo-phototronic effect. However, the performance enhancement of the p-n junction PD by the piezo-phototronic effect is much larger than that of the n-n junction PD. For the p-n junction PD, a photoresponsivity R of 14.5 A W^{-1} corresponding to an increase of 966 times, and a detectivity D^* of 1.65 × 10^{12} Jones corresponding to an enhancement of two orders of magnitude were obtained under an externally applied compressive strain of −0.50‰, accompanied by simultaneously improved response speed. On the other hand, for the n-n junction PD, a photoresponsivity R of 2.62 A W^{-1} with an enhancement of only 6 times, as well as a slightly improved detectivity D^* of 2.55 × 10^{11} Jones, was obtained under the same externally applied compressive strain. The different influences of the externally applied compressive strain on the two kinds of Si/CdS heterojunction PDs are due to the different energy band structures of the p-Si/n-CdS and n-Si/n-CdS junctions. These results provide a facile and effective way to enhance the photoresponse capability of Si-based materials in the NIR band by the piezo-phototronic effect, and in-depth understanding about the piezo-phototronic effect on the two different kinds of heterojunctions.

4. Experimental methods

4.1. Device fabrication process

First, the p- and n-type (100) silicon wafers (1–10 Ω cm, Universal Wafer) were etched in 5 wt% KOH solution with 5 vol% isopropanol at 85 °C for 30 min, and then the etched Si wafer with micron-scale tetrahedrons was ultrasonically cleaned for 5 min consecutively in acetone, distilled water and isopropanol. Next, a mixture solution of cadmium nitrate, thiourea, and glutathione (molar ratio of 1:1:0.6 with the concentration of cadmium nitrate as 15 mmol L^{-1}) was added to a 100 ml autoclave, and the etched Si wafer was placed into it with the growth surface facing down for CdS NW array growth. The autoclave was sealed and heated in an oven at 200 °C for 10 h,[34] and the products were cleaned with deionized water and vacuum-dried. Subsequently, a bottom electrode Al on Si and top electrode ITO on CdS NWs were deposited by RF magnetron sputtering (PVD75 system, Kurt. J. Lesker Co.), respectively. Finally, a thin layer of polydimethylsiloxane (PDMS) was spin-coated onto the top electrode to package the devices for making it optically transparent, flexible, and robust under externally applied compressive stress. The active area of the device for both of p-n and n-n junction was 2.25 mm^2.

4.2. Materials characterization and measurement

Microscopic structures of CdS NWs were characterized by SEM (Hitachi SU8010) and HRTEM (FEI F30). Transmission spectra of CdS were measured by a UV–visible spectrophotometer (JΛSCO V-630). The optical input stimuli were provided by a multi channel fiber coupled laser source (MCLS1, Thorlabs Inc.) with adjustable light power density, which was measured by a thermopile powermeter (Newport Model 1919-R). *I-V* characteristics measurements of the heterojunction NIR PDs were measured and recorded using a computer-controlled measurement system consisting of a Stanford SRS low noise current preamplifier (SR570)/SRS low noise voltage preamplifier (SR560) and a GPIB controller (GPIB-USB-HS, NI 488.2).

4.3. Calculations of external compressive strain and piezo-potential distribution

Through two layers of double-sided Kapton polyimide tape, we fixed the PD devices on a manipulation holder. An external compressive strain was applied onto the heterojunction PDs by uniformly pressing the surface of the device with a piece of transparent sapphire through a three-dimensional stage (moving resolution ~ 10 μm). The simulation dimensions are as follows: the bottom edge length and the height of the tetrahedrons are 5 and 3.5 μm, respectively. The diameter and length of CdS NWs, on average, are 50 nm and 600 nm, respectively. The thickness of PDMS layer is about 1.5 μm. Since the sapphire and silicon substrate are much stiffer than PDMS, their strains are negligible and thus ignored in this calculation. The elastic coefficient, piezoelectric coefficient, and relative permittivity matrices of CdS material and all the other materials' parameters used in the simulation are concluded in Tables S1 and S2 in Supporting Information, respectively. Finally, the piezoelectric constitutive equations are solved using the Solid Mechanics, Electrostatics and Piezoelectric Effect modules in COMSOL. After the computation, the average strains and piezo-potential distribution of the n-type CdS NWs under different compressive displacements could be derived and obtained by post-processing.

Acknowledgements

This research was supported by U.S. Department of Energy, Office of Basic Energy Sciences (Award DE-FG02-07ER46394) (the piezotronic and piezo-phototronic device fabrication and measurements), and the National Science Foundation (DMR-1505319) (materials synthesis and application in sensors).

Appendix A. Supporting information

Supplementary data associated with this article can be found in the online version at http://dx.doi.org/10.1016/j.nanoen.2017.11.076.

References

[1] L. Pavesi, D.J. Lockwood, Silicon Photonics: Silicon Fundamentals for Photonic Applications, Heidelberg, Berlin, 2004.
[2] K.D. Hirschman, L. Tsybeskov, S.P. Duttagupta, P.M. Fauchet, Nature 384 (1996) 338–341.
[3] X. Wang, Z. Cheng, K. Xu, H.K. Tsang, J.-B. Xu, Nat. Photon. 7 (2013) 888–891.
[4] O. Hayden, R. Agarwal, C.M. Lieber, Nat. Mater. 5 (2006) 352–356.
[5] Y.J. Hwang, A. Boukai, P. Yang, Nano Lett. 9 (2009) 410–415.
[6] C. Xie, X. Zhang, K. Ruan, Z. Shao, S.S. Dhaliwal, L. Wang, Q. Zhang, X. Zhang, J. Jie, J. Mater. Chem. A 1 (2013) 15348–15354.
[7] L. Pavesi, L. Dal Negro, C. Mazzoleni, G. Franzo, F. Priolo, Nature 408 (2000) 440–444.
[8] S. Pillai, K.R. Catchpole, T. Trupke, G. Zhang, J. Zhao, M.A. Green, Appl. Phys. Lett. 88 (2006) 161102.
[9] H. Rong, S. Xu, Y.-H. Kuo, V. Sih, O. Cohen, O. Raday, M. Paniccia, Nat. Photon. 1 (2007) 232–237.
[10] G. Konstantatos, E.H. Sargent, Nat. Nanotechnol. 5 (2010) 391–400.
[11] F. Guo, B. Yang, Y. Yuan, Z. Xiao, Q. Dong, Y. Bi, J. Huang, Nat. Nanotechnol. 7 (2012) 798–802.
[12] J.B.D. Soole, H. Schumacher, IEEE J. Quantum Electron. 27 (1991) 737–752.
[13] J.C. Campbell, J. Light. Technol. 25 (2007) 109–121.
[14] M.P. Hansen, D.S. Malchow, Proc. SPIE 6939 (2008) 69390I.
[15] F.H.L. Koppens, T. Mueller, Ph Avouris, A.C. Ferrari, M.S. Vitiello, M. Polini, Nat. Nanotechnol. 9 (2014) 780–793.
[16] Y. Wang, K. Ding, B. Sun, S.-T. Lee, J. Jie, Nano Res. 9 (2016) 72–93.
[17] D.J. Hall, L. Buckle, N.T. Gordon, J. Giess, J.E. Hails, J.W. Cairns, R.M. Lawrence, A. Graham, R.S. Hall, C. Maltby, T. Ashley, Appl. Phys. Lett. 85 (2004) 2113–2115.
[18] A. Sellai, P. Dawson, Nucl. Instrum. Methods A 567 (2006) 372–375.
[19] Z.L. Wang, J.H. Song, Science 312 (2006) 242–246.
[20] Y. Zhang, X. Yan, Y. Yang, Y. Huang, Q. Liao, J. Qi, Adv. Mater. 24 (2012) 4647–4655.
[21] Y. Zhang, Y. Yang, Y. Gu, X. Yan, Q. Liao, P. Li, Z. Zhang, Z. Wang, Nano Energy 14 (2015) 30–48.
[22] Z. Zhang, Q. Liao, Y. Yu, X. Wang, Y. Zhang, Nano Energy 9 (2014) 237–244.
[23] L. Zhu, L. Wang, C. Pan, L. Chen, F. Xue, B. Chen, L. Yang, L. Su, Z.L. Wang, ACS Nano 11 (2017) 1897–1900.
[24] C. Pan, M. Chen, R. Yu, Q. Yang, Y. Hu, Y. Zhang, Z.L. Wang, Adv. Mater. 28 (2016) 1535–1552.
[25] X. Liu, X. Yang, G. Gao, Z. Yang, H. Liu, Q. Li, Z. Lou, G. Shen, L. Liao, C. Pan, Z.L. Wang, ACS Nano 10 (2016) 7451–7457.
[26] X. Wang, R. Yu, C. Jiang, W. Hu, W. Wu, Y. Ding, W. Peng, S. Li, Z.L. Wang, Adv. Mater. 28 (2016) 7234–7242.
[27] Y. Dai, X. Wang, W. Peng, H. Zou, R. Yu, Y. Ding, C. Wu, Z.L. Wang, ACS Nano 11 (2017) 7118–7125.
[28] R.D.J. Vuuren, A. Armin, A.K. Pandey, P.L. Burn, P. Meredith, Adv. Mater. 28 (2016) 4766–4802.
[29] K. Sun, Y. Jing, N. Park, C. Li, Y. Bando, D. Wang, J. Am. Chem. Soc. 132 (2010) 15465–15467.
[30] S. Manna, S. Das, S.P. Mondal, R. Singha, S.K. Ray, J. Phys. Chem. C 116 (2012) 7126–7133.
[31] Y. Jiang, C. Li, W. Cao, Y. Jiang, S. Shang, C. Xia, Phys. Chem. Chem. Phys. 17 (2015) 16784–16790.
[32] Hamamatsu, silicon photodiodes series, ⟨http://www.hamamatsu.com/eu/en/product/category/index.html⟩, (Accessed October 2017).
[33] OSI Optoelectronics, silicon photodiodes series, ⟨http://www.osioptoelectronics.com/standard-products/default.aspx⟩, (Accessed October 2017).
[34] X. Liu, L.L. Gu, Q.P. Zhang, J.Y. Wu, Y.Z. Long, Z.Y. Fan, Nat. Commun. 5 (2014) 4007.
[35] S.M. Hatch, J. Briscoe, S. Dunn, Adv. Mater. 25 (2013) 867–871.
[36] Z. Wang, R. Yu, X. Wen, Y. Liu, C. Pan, W. Wu, Z.L. Wang, ACS Nano 8 (2014) 12866–12873.
[37] R. Bao, C. Wang, L. Dong, C. Shen, K. Zhao, C. Pan, Nanoscale 8 (2016) 8078–8082.
[38] S.M. Sze, CC/Eng. Tech. Appl. Sci. 27 (1982) 28.

Yejing Dai received her Ph.D. in Materials Science and Engineering from Tsinghua University in 2010. Now she is an associate professor at Tianjin University, China. Her main research interests focus on the fields of piezotronics/piezo-photonics, piezoelectric ceramics, and ceramic sintering behavior.

Xingfu Wang received his Ph.D. degree from South China Normal University (SCNU), with awards of Excellent Ph.D Dissertation, Top-ten Excellent Academic Paper in SCNU and National Scholarship for Graduate Students from Chinese Ministry of Education. From 2014–2017, he worked as a visiting scholar and research engineer in Prof. Zhong Lin Wang's group at Georgia Tech. He now is a professor, Outstanding Young Scholar at SCNU, Guangzhou, China. His research interests include epitaxial growth of III-Nitride planar/nano-structures by Metal-Organic Chemical Vapor Deposition (MOCVD); GaN-based light-emitting-diode (LEDs) and high-electron-mobility-transistor (HEMTs); Piezotronics/Piezo-photonics.

Dr. Wenbo Peng received his Ph.D. in Electronics Science & Technology and BS in Microelectronics from Xi'an Jiaotong University, China in 2016 and 2010. From Aug 2014 to Aug 2016, he has been a visiting Ph.D. student in School of Materials Science and Engineering at Georgia Institute of Technology under the supervision of Prof. Zhong Lin (Z. L.) Wang supported by the program of China Scholarship Council. Now he is an Assistant Professor in School of Microelectronics in Xi'an Jiaotong University. His research interests mainly focus on piezotronics/piezo-phototronics, tribotronics, surface acoustic wave sensors, and triboelectric nanogenerators.

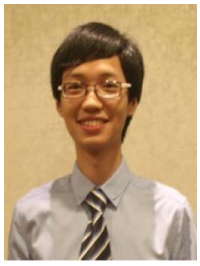

Changsheng Wu received his Bachelor of Engineering in Engineering Science Programme from National University of Singapore in 2013. He is currently pursuing a Ph.D. in Materials Science and Engineering at Georgia Institute of Technology under the supervision of Prof. Zhong Lin Wang. His research interests include energy harvesting, self-powered electroncis and additive manufacturing.

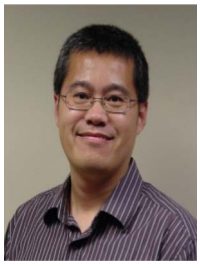

Dr. Yong Ding is a senior research engineer at Georgia Tech. He received his Ph.D. degree in physics from Nanjing University in 2012. His research interests mainly focus on the applications of transmission electron microscopy in materials science.

Kai Dong received his M.S. degree in Textile Materials and Design from Donghua University (Shanghai, China, 2013–2015) and B.S. degree in Textile Materials and Design from Yanchen Institute of Technology (Jiangsu, China, 2009–2013). He started to pursue his Ph.D. degree in College of Textile at Donghua University in 2015. Now he is a visiting Ph.D. student in the Materials Science and Engineering at Georgia Institute of Technology through the program of China Scholarship Council (CSC). His research focuses primarily on textile-based triboelectric nanogenerator, energy harvesting/storage, self-powered sensor, wearable electronics, thermal conductivity, textile composites.

Zhong Lin (ZL) Wang received his Ph.D. from Arizona State University in physics. He now is the Hightower Chair in Materials Science and Engineering, Regents' Professor, Engineering Distinguished Professor and Director, Center for Nanostructure Characterization, at Georgia Tech. Dr. Wang has made original and innovative contributions to the synthesis, discovery, characterization and understanding of fundamental physical properties of oxide nanobelts and nanowires, as well as applications of nanowires in energy sciences, electronics, optoelectronics and biological science. His discovery and breakthroughs in developing nanogenerators established the principle and technological road map for harvesting mechanical energy from environment and biological systems for powering personal electronics. His research on self-powered nanosystems has inspired the worldwide effort in academia and industry for studying energy for micro-nano-systems, which is now a distinct disciplinary in energy research and future sensor networks. He coined and pioneered the field of piezotronics and piezo-phototronics by introducing piezoelectric potential gated charge transport process in fabricating new electronic and optoelectronic devices. Details can be found at: http://www. nanoscience.gatech.edu.